Hysteretic Behavior of Concrete Masonry Shear Walls with Unbonded Reinforcement

Alok Madan[1], Andrei M. Reinhorn[2], John B. Mander[3]

In reinforced concrete masonry shear walls with ungrouted cells, the longitudinal steel reinforcing bars are not bonded (unbonded) to the neighboring masonry. As a result, the steel strains as well as forces are governed by the relative displacements of the end anchorages and are, therefore, dependent on the deformations of the entire wall. After the development of the first flexural crack at the base, the in-plane lateral load is resisted primarily by arch action (tie-strut mechanism) due to the absence of bonding in such walls, as opposed to beam action which is the dominant load resisting mechanism for shear walls with bonded reinforcement. Further, the flexural cracking causes a partial loss of connectivity at the base, thus, introducing, in addition to the in-plane flexural and shear deformations, an uplift or separation of the wall from the foundation at one end. Repeated reversals of the in-plane lateral load result in consecutive opening and closing of the separation at the base. Since the unbonded longitudinal reinforcement cannot resist compression effectively due to absence of bracing along the wall height, cyclic load reversals generate a 'rocking' type of motion in the wall in some cases, thus resulting in 'pinching' of force-displacement hysteresis curves into 'S' shaped loops which are characteristic of this class of structural walls. Because of these peculiarities, the presently available analytical models for reinforced masonry elements are deficient for estimating the hysteretic behavior of masonry shear walls with ungrouted longitudinal (vertical) reinforcement under reversed cyclic loading.

An extensive review of literature on the state-of-the-art modeling of ungrouted post-tensioned and reinforced masonry shear walls (with unbonded vertical reinforcement) is presented by Madan et al. (1996). An additional review of the subsequent literature indicates that there is a need for analytical modeling and design guidelines for evaluation of hysteretic performance of such walls. The existing analysis techniques for reinforced masonry or concrete structures are inadequate for predicting the hysteretic response of masonry shear walls with unbonded longitudinal reinforcement under cyclic load reversals. Moreover, the engineering design formulations based on the available analytical models for reinforced masonry and concrete are deficient for reliable estimation of the lateral in-plane force-displacement response parameters of these walls in the nonlinear range of behavior (such as strength, ductility and post-yield stiffness). More rigorous analytical models need to be developed for this purpose which account for the absence of bond between the vertical steel reinforcement and masonry using force equilibrium and displacement compatibility [Madan (1996), Madan et al. (1996)].

In unreinforced masonry shear walls subjected to an in-plane lateral load, subsequent to the formation of a flexural crack at the base, a part of the base may separate from and lift off the foundation if the applied overturning moment exceeds the restoring moment. In the case of reinforced masonry walls with bonded reinforcement, the bonding between the steel and masonry restrains this uplift. The uplift, which is governed by external forces and inertial effects, causes a local increase in stresses in the region of contact between the wall base and foundation due to reduction in contact area. As the contact area reduces further with progressive uplift, the stresses may become inelastic resulting in a non-linear response. At the same time, the external loads produce in-plane flexural and shear deformations in the flexible wall body. The modeling of the uplift phenomenon may be simplified by assuming that the strain deformations are limited to the wall base-foundation contact surface, thus, considering the wall body to be rigid [Priestley (1991)]. However, this assumption may be erroneous in the range where the applied overturning moment is less than the overturning capacity of the walls. In that case, the response will be dominated by the flexural and shear deformations of the entire wall. In case of masonry shear walls reinforced with unbonded reinforcement, the problem is complicated by the fact that the reinforcing bars exert tie-down or restoring forces on the wall which depend on the displacements of the entire wall [Madan et al. (1996)]. A review of state-of-the-art methods for analyzing the response of flexible structures rocking on a flexible foundation indicates that the available analytical models for predicting the force-displacement envelope of such structures undergoing strain deformations along with uplift are based on simplifying idealizations such as assuming a rigid wall body on an elastic plastic foundation [Priestley (1991)], representing the flexible foundation by distributed Winkler springs [Badawi (1989), Housner (1957)] which are effective only in compression (for modeling the non-linear contact problem) or adding a rigid body rotational degree of freedom about the center of the base [Housner (1957),

[1] Assistant Professor, Department of Civil Engineering, Indian Institute of Technology, New Delhi, India
[2] Professor, Department of Civil Engineering, State University of New York, Buffalo, NY 14260
[3] Associate Professor, Department of Civil Engineering, State University of New York, Buffalo, NY 14260

Haroun (1980), Haroun et al. (1981), Haroun et al. (1985), Natsiavas(1988), Natsiavas et al. (1988), Yi et al. (1992)] which may be unrestrained or restrained by appropriate rotational springs or dampers or both. There is a need for rigorous analytical formulations that realistically model the non-linear stress distribution at the ground-structure interface resulting from uplift of the base.

A micro element model is presented in this paper for predicting the nonlinear hysteretic behavior of masonry shear walls with ungrouted longitudinal reinforcement accounting for the interaction of flexure and uplift under lateral in-plane cyclic loading. An analysis procedure is developed for evaluating the hysteretic in-plane lateral force-displacement response of masonry shear walls with unbonded longitudinal reinforcement subjected to reversed cyclic loading in the inelastic range of behavior. The formulation of the analytical procedure is completed assuming cantilever boundary conditions for the shear wall and a concentrated lateral load at the free end. As a result, the model is applicable in the present form only to such cantilever walls. However, the model can be extended for other boundary conditions by altering the analytical formulation suitably. The proposed analytical model was used to predict the experimental force-displacement hysteresis behavior of wall specimens tested under lateral in-plane cyclic loading, as part of the experimental evaluation in a research program based on investigation of in-plane behavior of masonry shear walls with unbonded vertical reinforcement with or without prestress. The present paper is part of a series based on the results of the research program.

BACKGROUND

An analysis technique was presented by Madan et al. (1996) for predicting the monotonic inelastic flexural moment-curvature response of masonry shear walls with unbonded vertical reinforcement. The technique was based on a modified fiber element model (micro element model) in which the masonry wall is discretized into a finite number of sections along the height and each of these finite sections is discretized into a finite number of fibers along the section length. The modified fiber model proposed by Madan et al. (1996) was extended in this development for analyzing the cyclic in-plane force-displacement behavior of masonry shear walls with unbonded vertical reinforcement. A brief review of the previously proposed modified fiber model for flexural behavior of masonry shear walls with unbonded vertical reinforcement [Madan et al. (1996)] is included in this section with the purpose of providing the necessary background for further development and completeness.

Consider the inelastic flexural response analysis of a reinforced concrete masonry shear wall [Figure 1(a)] of height H, width b and length L under the action of an in-plane lateral load V_y applied at the top of the wall with n_b number of reinforcing bars of cross-sectional areas A_{sj} located at coordinates y_j from the center of wall section [Figure 1(d)], where the subscript j refers to the j^{th} bar. The axial force $P_x(x_i)$ and the bending moment $M_z(x_i)$ at any discrete section i at height x_i from the base can be statically determined and their variations along the wall height are shown in Figures 1(b) and 1(c) respectively. The inelastic flexural response of the masonry shear wall may be analyzed using common assumptions such as:

(a) The strain distribution in masonry at any given section varies linearly along the depth i.e. plane sections remain plane, which is a realistic representation of physical behavior for shear walls with large aspect ratios (ratio of height H to length L).
(b) The uniaxial stress-strain relationships for masonry and steel are known.
(c) The widths of discrete cracks in masonry are considered smeared along the height of the wall i.e. a "smeared crack model" of the wall is used. The assumption does not allow the determination of local conditions (e.g. local curvatures) at the discrete crack locations. However, the smeared crack modeling is a widely accepted pragmatic approach that is efficient yet accurate for the purpose of evaluating average moment-curvature relationship over a large span (height in this case) and, therefore, the global or overall flexural response of the wall.

Assumption (a) implies that the longitudinal masonry strain $\varepsilon_x(x_i)$ in any section i at coordinate y from the center may be calculated as:

$$\varepsilon_x(x_i, y) = \xi(x_i) + y\,\Phi(x_i) \quad \textbf{(1)}$$

where $\xi(x_i)$ is the strain in masonry at the center of the ith section and $\Phi(x_i)$ is the angle of inclination of the linear strain profile at the i^{th} section also known as the curvature at that section [Figure 1(e)].

Evidently, at any section i, there are 2 unknown masonry strain variables (the masonry strain at the center of wall section $\xi(x_i)$ and the curvature $\Phi(x_i)$ of the section) and n_b unknown steel strain variables (the strains $\varepsilon_s(x_i, y_i)$ in each of the steel rebars). To solve for these unknown strain variables, two equations are available at each section from the force and moment equilibrium of the section. The force and moment equilibrium of the i^{th} section may be written as:

$$P_x(x_i) = C(x_i) - T_s(x_i) \quad \textbf{(2)}$$

$$M_z(x_i) = M(x_i) - M_s(x_i) \quad \textbf{(3)}$$

where $C(x_i)$ are the internal compressive forces in masonry and $T_s(x_i)$ are the internal tensile forces in steel in the axial

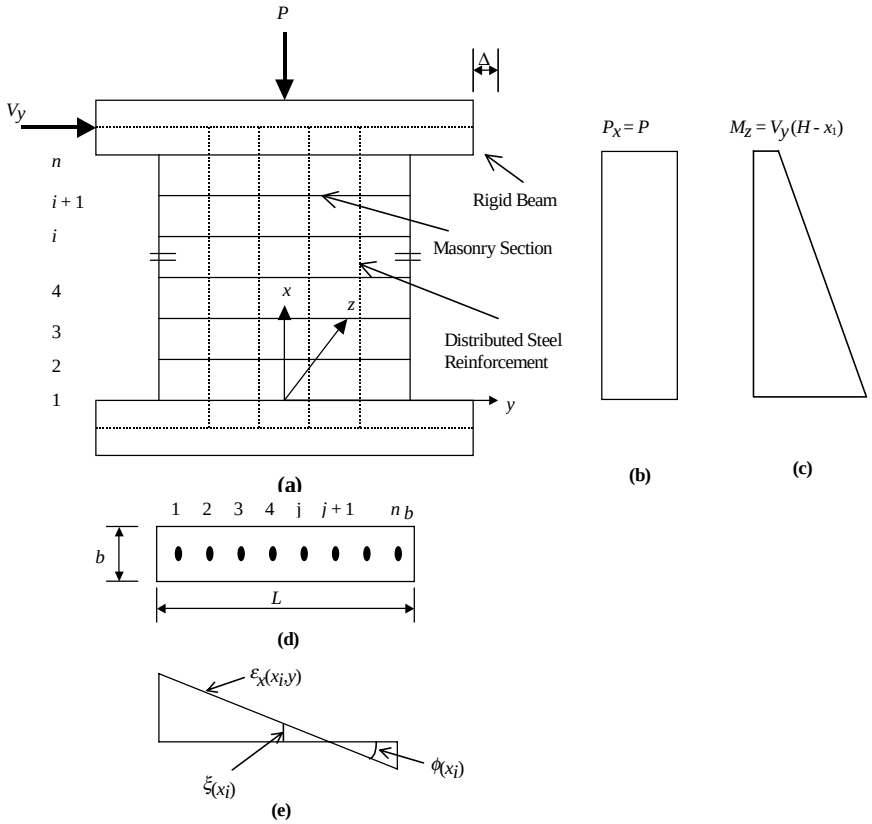

Figure 1—Concrete Masonry Shear Wall with Distributed Vertical Reinforcement

direction which are calculated as:

$$C(x_i) = C\left[\xi(x_i),\ \Phi(x_i)\right] = \int_{-L/2}^{L/2}\left[\xi(x_i) + y\,\Phi(x_i)\right]E_m\left[\xi(x_i) + y\,\Phi(x_i)\right]b\,dy \quad \textbf{(4a)}$$

$$T(x_i) = \sum_{j=1}^{n_b} E_s(\varepsilon_s)\,A_{sj}\,\varepsilon_s(x_i, y_j) \quad \textbf{(4b)}$$

and $M(x_i)$ and $M_s(x_i)$ are the internal in-plane resisting moments due to masonry and steel respectively at the section and, are calculated as:

$$M(x_i) = M\left[\xi(x_i),\ \Phi(x_i)\right] = \int_{-L/2}^{L/2} y\left[\xi(x_i) + y\,\Phi(x_i)\right]E_m\left[\xi(x_i) + y\,\Phi(x_i)\right]b\,dy \quad \textbf{(5a)}$$

$$M_s(x_i) = \sum_{j=1}^{n_b} E_s(\varepsilon_s)\,A_{sj}\,\varepsilon_s(x_i, y_j) \quad \textbf{(5b)}$$

in which, $E_m(\varepsilon_m)$ and $E_s(\varepsilon_s)$ are the masonry and steel stress-strain relationships, respectively.

In ungrouted reinforced concrete masonry shear walls (i.e. with unbonded longitudinal reinforcement), the absence of bonding between longitudinal steel and surrounding masonry does not permit the assumption of local strain compatibility between steel and masonry at any section. In any case, however, the displacement of the anchored end of any unbonded reinforcing bar at top or bottom of the wall must equal the displacement of the masonry section at that location. The lack of bond implies that the strain in the rebar remains constant along the height of the wall, i. e.,

$$\varepsilon_s(y_j) = \varepsilon_s(x_1, y_j) = \ldots = \varepsilon_s(x_i, y_j) = \varepsilon_s(x_{i+1}, y_j) = \ldots = \varepsilon_s(x_n, y_j) \quad \textbf{(6)}$$

Additionally, displacement compatibility at the wall boundary requires that the total extension of the rebar over the height H between the anchorages must equal the total elongation of the masonry fiber at that location [Park and Paulay (1975)]. Thus, the component of strain in the j^{th} rebar due to flexural deformations $\varepsilon_{sf}(y_i)$ may be calculated from the aforementioned compatibility criteria as follows:

$$\varepsilon_{sf}(y_j) = \varepsilon_p + \frac{\int_0^H \varepsilon_x(x, y_j)\,dx}{H} = \varepsilon_p + \frac{\int_0^H \left[\xi(x) + y_j\,\Phi(x)\right]dx}{H} \quad \textbf{(7)}$$

where ε_p is the original prestressing strain in the reinforcing bars (if such prestressing is applied).

The foregoing review makes it evident that the flexural response of concrete masonry shear walls with unbonded reinforcement is indeterminate at the sectional level [Madan et al. (1996)]. The displacement compatibility between masonry and reinforcing steel at the location of end anchorages on the wall boundary [Equation 7] provides the necessary and sufficient condition for unique solution of the unknown flexural strain variables. Detailed formulation of the numerical solution technique is presented by Madan et al. (1996) for obtaining the flexural moment-curvature response at each of the discrete sections along the height in a masonry shear wall with unbonded reinforcement under the action of monotonic in-plane lateral loading. The in-plane lateral force and displacement corresponding to the flexural curvatures of the masonry shear wall may be calculated by idealizing the top of the wall as a free end and the base as a fixed end (cantilever end conditions). Thus, the lateral force V_y applied at height H above the base of the wall equals the shear force at any section i along the height of the wall and may be calculated as:

$$V_y = V(x_1) = V(x_2) = \ldots = V(x_i) = \ldots = V(x_n) = M_z(x_i) / (H - x_i) \quad \textbf{(8)}$$

The lateral displacement at the top of the wall due to flexural deformations may be obtained by integrating the curvatures along the height as:

$$f = \int_0^H \Phi(x)\,(H - x)\,dx \quad \textbf{(9)}$$

The authors wish to note here that Equation 8 is valid only for a cantilever wall with a concentrated lateral load at the free end of the wall. Further, Equation 9 is inadmissible for any other set of boundary conditions. Thus, the analytical procedure presented in this paper is applicable only to cantilever walls with a lateral load at the free end. For other boundary and loading conditions, the formulation will have to be modified by replacing Equations 8 and 9 with the appropriate statical and kinematic relationships respectively.

ANALYTICAL MODELING OF HYSTERETIC FORCE-DISPLACEMENT RESPONSE

In reinforced concrete masonry shear walls with ungrouted vertical reinforcement, the formation of a flexural crack at the base causes a loss of connectivity, thus, resulting in a separation or uplift of the wall base from the foundation at one end. In walls with grouted reinforcement, this uplift is restrained by the bond between the vertical reinforcing bars (anchored into the foundation) and the adjoining concrete. The uplift of the base introduces yet another unknown degree of freedom to the wall in addition to the flexural strain variables. Since the modified fiber model was originally proposed for flexural moment-curvature analysis under monotonic loading [Madan et al. (1996)], the analytical model needs to be expanded to account for uplift and cyclic load reversals for the purpose of developing an analysis procedure for predicting the in-plane hysteretic force-displacement behavior of the wall. The modified fiber model was complemented in the present development with a theoretical model for estimating the uplift displacements. Additionally, cyclic constitutive models of the component materials, i.e., masonry and steel were implemented for analysis of hysteretic response under reversed cyclic loading. Since the proposed analysis procedure is based on a model of flexural behavior, the shear deformations of the wall are inherently neglected by the analysis.

Modeling of Uplift

In masonry walls with unbonded reinforcement, flexural cracking at the base results in a partial loss of fixity at the base thus causing a part of the base to uplift off the foundation. Under these conditions, a rigid body motion coexists with the flexural and shear response (strain deformations). Since the strains in the unbonded reinforcing bars depend on the relative displacements of the end anchorages [Park and Paulay (1975)], the steel strains are functions of strain deformations as well as uplift displacements of the wall. The degree to which the wall undergoes rigid body motion in comparison to the strain deformations at any time of loading depends on various parameters such as the overturning moment at base $M_z(x_1)$, time rate of change of the overturning moment, wall aspect ratio or height to length H / L ratio, axial load $P_x(x_1)$ at the base, prestress in the vertical unbonded rebars $\varepsilon_p(y_j)$ and wall weight W. The exact dependence of the magnitude of rigid body motion on these parameters is a complex kinematic phenomenon. Intuitively, however, progressive uplift of the wall base causes a reduction in the area of contact between the base and foundation thus producing a stress concentration in the contact region. Therefore, there exists a compatibility between the magnitude of base uplift or rigid body motion and the strains at the base. The following assumptions were made in this formulation to model the uplift or rocking response of the masonry shear walls with unbonded vertical reinforcement:

1. Subsequent to the formation of flexural crack at the base, a rigid body rotation θ of the shear wall (Figure 2) occurs along with the strain deformations as a result of lateral loading. The instantaneous center of this rigid body rotation was assumed at the point of action of the resultant of compressive stress distribution (i.e. the point of reaction C) at the base.
2. The incremental strain displacement $\partial\delta_c$ at the wall toe (extreme compression fiber) can be related to the incremental angle of uplift $\partial\theta_\delta$ between the uplifted base and foundation at the point of separation (Figure 2).
3. The incremental strain displacement $\partial\delta_c$ at the extreme

compression fiber (toe) can be averaged over a finite height H_p to obtain the incremental compressive normal strain at that location $\partial\varepsilon_x(x_1, L/2)$. The height H_p will be referred to in this study as the average height of the stressed zone and its value depends on the parameters that govern rigid body motion which have been mentioned earlier.

Using the foregoing assumptions, a compatibility condition is derived between the rigid body rotation θ of the wall and curvature $\phi(x_1)$ at the base. The proposed compatibility relation is based on the wall length L, contact length d between the base and foundation, distance d_c of centroid of the compressive stress distribution (point of reaction) at base from the extreme compression fiber (toe of the wall), the average height H_p of the stressed zone. Referring to Figure 2, the following relation may be obtained at any stage of loading from geometry:

$$\partial\delta = \frac{(L-d)}{(L-d_c)}\partial\theta_\delta \qquad \textbf{(10)}$$

Using assumption 2 above and Figure 2, the following relation is proposed:

$$\partial\theta_\delta = \frac{\partial\delta_c}{d} = \frac{\partial\delta_t}{(L-d)} \qquad \textbf{(11)}$$

From assumption 3 above, the curvature at base $\phi(x_1)$ may be related to the strain displacement at the extreme compression fiber as follows:

$$\partial\Phi(x_1) = \frac{\partial\varepsilon_x(x_1, L/2)}{d} = \frac{\partial\delta_c}{H_p\, d} \qquad \textbf{(12)}$$

Thus, from the above assumptions, using Equations 10, 11 and 12, the following compatibility condition can be written between the rigid body rotation θ of the wall and base curvature $\phi(x_1)$:

$$\partial\theta = 0; \qquad \text{if} \quad \varepsilon_x(x_1, -L/2) \geq \varepsilon_{cr} \qquad \textbf{(13a)}$$

$$\partial\theta = \frac{H_p(L-d)}{(L-d_c)}\partial\Phi(x_1); \text{ if} \quad \varepsilon_x(x_1, -L/2) < \varepsilon_{cr} \qquad \textbf{(13b)}$$

in which, ε_{cr} is the cracking strain for masonry and d is the instantaneous contact length at the base which may be estimated as:

$$d = \frac{L}{2} + \frac{\xi(x_1)}{\Phi(x_1)} \qquad \textbf{(14)}$$

The instantaneous location of the resultant C of the compressive stress distribution at the base may be calculated from mechanics as:

$$y_c = \frac{M(x_1)}{C(x_1)} \qquad \textbf{(15)}$$

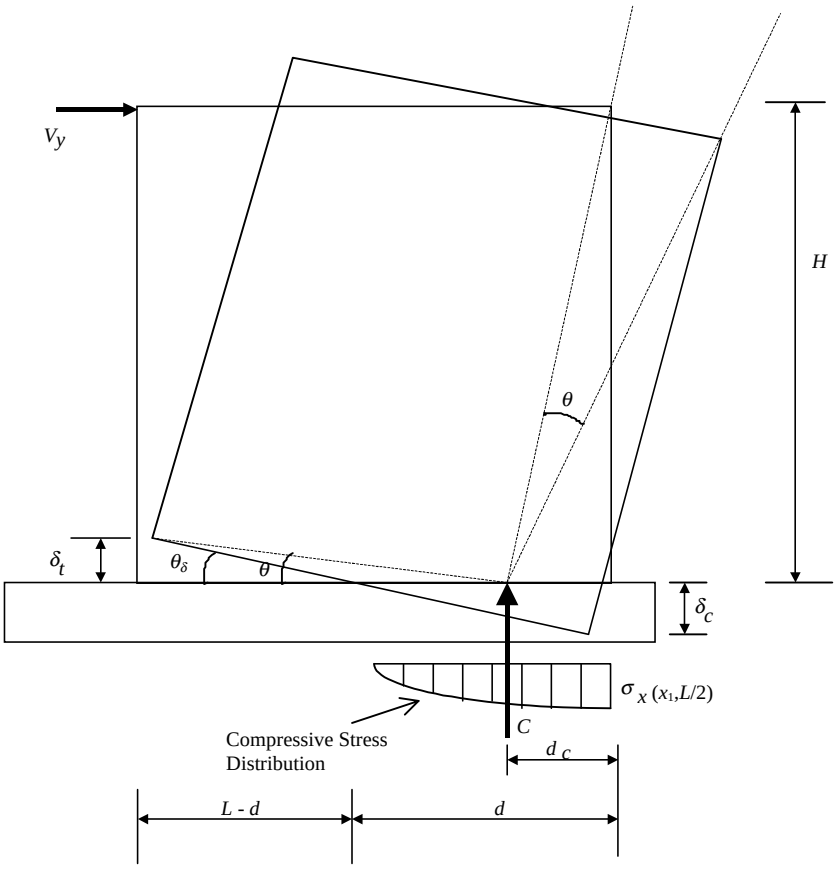

Figure 2: Displacement Compatibility of Wall Uplift in Masonry Walls

in which y_c is y coordinate of the point of action of compressive stress resultant C. Thus, the distance d_c of the compressive stress resultant from the extreme compression fiber (toe of the wall) is obtained as:

$$d_c = \frac{L}{2} - y_c = \frac{L}{2} - \frac{M(x_1)}{C(x_1)} \quad \textbf{(16)}$$

The lateral in-plane displacement $v_r(x,y)$ due to uplift or rocking response may be estimated using small angle approximation as:

$$v_r(x, y) = \theta\, x \quad \textbf{(17)}$$

Using assumption 1, the vertical in-plane displacement $u_r(x,y)$ due to uplift may be approximated as:

$$u_r(x, y) = \theta(y_c - y) = \theta\left[\frac{M(x_1)}{C(x_1)} - y\right] \quad \textbf{(18)}$$

The lateral in-plane displacement Δ_r at the top leeward edge $(x = H, y = L/2)$ due to uplift or rocking response may be obtained from Equation 17 as:

$$\Delta_r = v_r(H, L/2) = \theta H \quad \textbf{(19)}$$

The total lateral in-plane displacement Δ is obtained by adding the component due to flexure from Equation 9 as:

$$\Delta = \Delta_f + \Delta_r = \int_0^H \Phi(x)(H - x)\,dx + \theta H \quad \textbf{(20)}$$

The vertical in-plane displacement $U_r(y_j)$ of the n^{th} section at the location of the j^{th} reinforcing bar due to wall uplift may be calculated using Equation 18 as:

$$U_r(y_j) = \theta(y_c - y_j) = \theta\left[\frac{M(x_1)}{C(x_1)} - y_j\right] \quad \textbf{(21)}$$

Assuming that lower anchorage of the wall is stationary, the relative longitudinal displacement of the upper anchorage with respect to the lower one due to uplift can be approximated as the vertical in-plane displacement $U_r(y_j)$ above. Thus, the uniaxial longitudinal strain component $\varepsilon_{sr}(y_j)$ in the j^{th} rebar due of uplift may be obtained as:

$$\varepsilon_{sr}(y_j) = \frac{U_r(y_j)}{H} = \frac{\theta\left[\frac{M(x_1)}{C(x_1)} - y_j\right]}{H} \quad \textbf{(22)}$$

The total longitudinal strain in j^{th} rebar $\varepsilon_s(y_j)$ is obtained by adding the strain component due to flexure and prestressing from Equation 7 as follows:

$$\varepsilon_s(y_j) = \varepsilon_{sf}(y_j) + \varepsilon_{sr}(y_j) = \varepsilon_p + \frac{\int_0^H \left[\xi(x_i) + y_j\,\Phi(x_i)\right]dx}{H} + \frac{\theta\left[\frac{M(x_1)}{C(x_1)} - y_j\right]}{H} \quad \textbf{(23)}$$

in which ε_p is the strain due to prestress in the rebars.

Cyclic Constitutive Models

The analysis of lateral in-plane hysteretic force-displacement response of the masonry shear wall under cyclic load reversals requires specification of cyclic stress-strain rules for masonry and steel. A piece-wise linear stress-strain envelope shown in Figure 3(a) was specified for masonry in uniaxial compression. The compressive stress-strain envelope consists of a bilinear ascending part to model the decreasing stiffness as the stress f_m increases to the peak compressive strength f'_m. After attaining the peak value, the stress was assumed to drop linearly to a control stress-strain point. At higher strains, the stress was assumed to remain constant at a specified value until the crushing strain is reached. At this point, the masonry stress goes to zero and the masonry fiber is assumed to fail in compression. The tensile stress-strain envelope was assumed to be linearly elastic for stresses until the cracking strength (f_{cr}) is reached. For higher tensile strains, the stress in the fiber is assumed to be zero and tensile failure is assumed. The elastic stiffness of the tensile stress-strain envelope was assumed the same as the initial slope of the compressive stress-strain envelope. A linear stress-strain relationship was assumed for the masonry fibers during unloading and reloading. The unloading branches of the stress-strain curve were assumed to converge to a specified control point ε_o on the tensile strength envelope. In any case, the stiffness or slope of the linear unloading branch was constrained to be less than the initial stiffness of the stress-strain envelope. The slope of the reloading branch was assumed equal to the initial slope of the strength envelope.

A bilinear elastic-perfectly plastic stress-strain envelope was defined for the longitudinal steel reinforcing bars. The slopes of both the unloading and reloading branches were assumed equal to the initial elastic stiffness of the envelope. Thus, a cyclic elastic-perfectly plastic constitutive law illustrated in Figure 3(b) was specified for steel. A different value of yield stress may be specified for tension (f_{yt}) and compression (f_{yc}) for the sake of generalization. In reality, reinforcing steel exhibits significant strain hardening, however, as the longitudinal steel yields over its entire length, the plastic strains tend to be modest - generally less than 3 percent. Therefore, an elastic-plastic model for the steel stress-strain behavior is justified. In any case, the proposed analysis method is sufficiently flexible to allow the implementation of more general stress-strain models.

Numerical Solution of Hysteretic Response

A numerical solution technique was proposed by Madan et al. (1996) based on the modified fiber model for analyzing the inelastic flexural response of concrete masonry shear walls with unbonded reinforcement under the action of a monotonic in-plane lateral load. The proposed method involves discretization of the wall into a finite number of

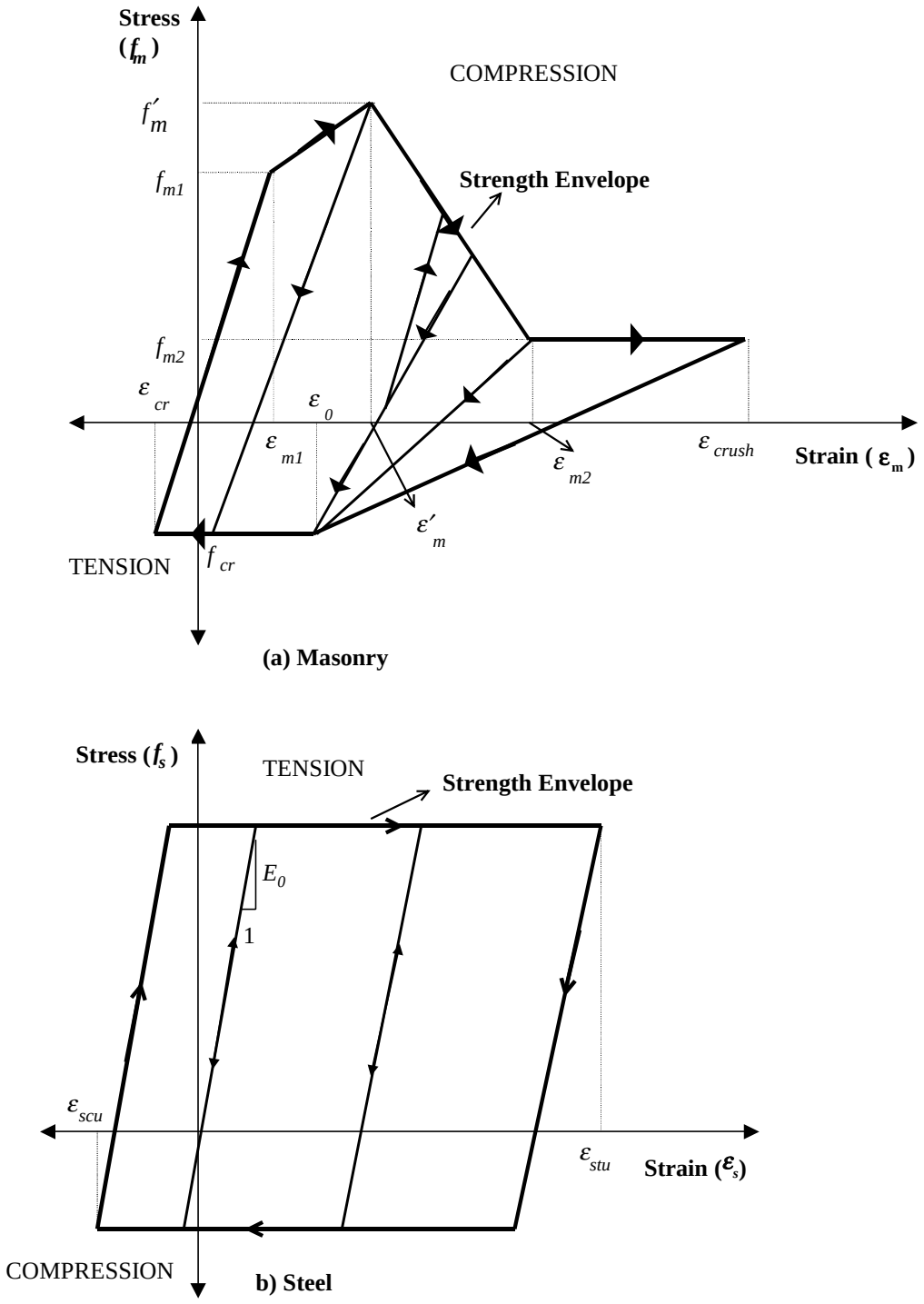

Figure 3— Cyclic Material Constitutive Models for Masonry and Concrete

sections *n* along the height [Figure 1(a)]. Since the strains in the unbonded rebars do not vary along height of the wall, the internal steel force $T_s(x_i)$ and moment $M_s(x_i)$ also remain constant for all the *n* sections. In mathematical terms, from Equations 4(b), 5(b) and (6):

$$T_s(x_i) = T_s = \sum_{j=1}^{n_b} E_s(\varepsilon_s) A_{sj}\, \varepsilon_s(y_j) \qquad \textbf{(24)}$$

$$M_s(x_i) = M_s = \sum_{j=1}^{n_b} E_s(\varepsilon_s) A_{sj}\, y_j\, \varepsilon_s(y_j) \qquad \textbf{(25)}$$

The numerical technique is based on the idealization that internal action of the unbonded steel reinforcing bars is statically equivalent to a structural force T_s given by Equation (24) and a structural moment M_s given by Equation (25) that are unknown and depend on kinematics of the structural masonry wall [Madan et al. (1996)].

The numerical solution methodology was augmented in the present development to incorporate the effect of uplift and cyclic load reversals for analyzing the hysteretic in-plane lateral force-displacement response of the masonry wall under cyclic displacement control. A flowchart of the extended solution algorithm is presented in Figure 4. The solution procedure involves an iterative scheme which begins by assuming the unknown steel force T_s and moment M_s for a given control curvature at the base. For the assumed value of the steel force, the unknown masonry strain $\xi(x_i)$ is computed at the base section ($i = 1$) using the sectional force equilibrium equation [Equation (2)]. The algorithm then computes the external moment at the base $M_z(x_1)$ using sectional moment equilibrium equation [Equation (3)] which in turn statically determines the external moment $M_z(x_i)$ at all the other finite sections $i = 2$ to n. The algorithm then proceeds to compute the sectional masonry strain variables $\xi(x_i)$ and $\Phi(x_i)$ at each finite section above the base ($i = 2$ to n) using sectional force and moment equilibrium equations [Equations (2) and (3)]. The solution of the sectional force and moment equilibrium equations is obtained using the Newton-Raphson method. The internal masonry force $C(x_i)$ and moment $M(x_i)$ for the i^{th} section are numerically integrated from the masonry strain variables $\xi(x_i)$ and $\Phi(x_i)$ by discretizing the section into n_f number of fibers each of thickness t_k along the in-plane length of the wall where the subscript k refers to the k^{th} fiber. Therefore, for given values of the strain variables $\xi(x_i)$ and $\Phi(x_i)$ at any section i, the masonry force and moment at that section can be calculated using Equations 4(a) and 5(a) as follows:

$$C\left[\xi(x_i), \Phi(x_i)\right] = \sum_{k=1}^{n_f}\left[\xi(x_i) + y_k\ \Phi(x_i)\right] E_m \left[\xi(x_i) + y_k\ \Phi(x_i)\right] b\, t \qquad \textbf{(26)}$$

$$M\left[\xi(x_i), \Phi(x_i)\right] = \sum_{k=1}^{n_f} y_k\left[\xi(x_i) + y_k\ \Phi(x_i)\right] E_m \left[\xi(x_i) + y_k\ \Phi(x_i)\right] b\, t_k \qquad \textbf{(27)}$$

Detailed flowcharts for the numerical solution of the sectional equilibrium equations are presented by Madan et al. (1996).

Subsequent to the determination of the sectional masonry strain variables at all the discrete sections, the rigid body rotation θ due to uplift is estimated using Equation 13. Henceforth, the strains in the reinforcing bars $\varepsilon_s(y_j)$ are computed using the compatibility Equation 23. From the steel strains, the stresses in the unbonded reinforcing bars can be calculated using the prescribed cyclic constitutive rule for steel. The steel stresses in turn provide the forces in the rebars which are summated to compute a new estimate of the steel force T_s and moment M_s. The computed steel force and moment are compared with the assumed values. In case the errors are more than the allowable tolerances, T_s and M_s are revised and the analysis is repeated until the assumed values converge with the computed values. Upon convergence, the in-plane lateral force is calculated from Equation 8 while the lateral displacement at the top of the wall is obtained from Equation 20 by numerically integrating the curvatures along the height as:

$$\Delta = \Delta_f + \Delta_r = \sum_{i=1}^{n} \hat{w}_i\ \Phi(x_i)\,(H - x_i)\,\delta x_i + \theta\, H \qquad \textbf{(28)}$$

where $\hat{w}_i$, is a constant for numerical integration.

Modification for Analysis of Masonry Shear Walls with Bonded Reinforcement

The proposed analysis procedure can be easily adapted for evaluating the hysteretic response of masonry shear walls with bonded (i. e. grouted) longitudinal reinforcement as a special case. In this case, the strains in the vertical reinforcing bars can be directly related to the masonry strain variables $\xi(x_i)$ and $\Phi(x_i)$ at each finite section using the following compatibility equation for bonded reinforcement:

$$\varepsilon_s(x_i, y_j) = \varepsilon_x(x_i, y_j) = \xi(x_i) + y_j\ \Phi(x_i),\quad j = 1, n_b \qquad \textbf{(29)}$$

Therefore, the steel force T_s and moment M_s can be calculated and iterated independently for each finite section to obtain the inelastic flexural response at that section for a given control curvature at the base.

EXPERIMENTAL VERIFICATION

An experimental study was performed to evaluate the in-plane seismic response of masonry shear walls with unbonded reinforcement [Madan (1996)]. Six shear wall specimens were tested as part of the experimental program for the purpose of investigating the influence of various parameters including axial load, lateral drift amplitudes, prestressing, shear deformations and reinforcement anchorage on the in-plane seismic behavior. Wall Specimens 2, 3 and 4 were designed to display a predominant flexural mode of failure under lateral in-plane loading. The proposed analysis technique was used to predict the hysteresis behavior observed during the testing of these wall specimens under reversed cyclic loading. The details of the test specimens are illustrated in Figure 5. The salient test parameters and results for these specimens are presented in Table 1. Further details of the test program may be found elsewhere [Madan (1996)].

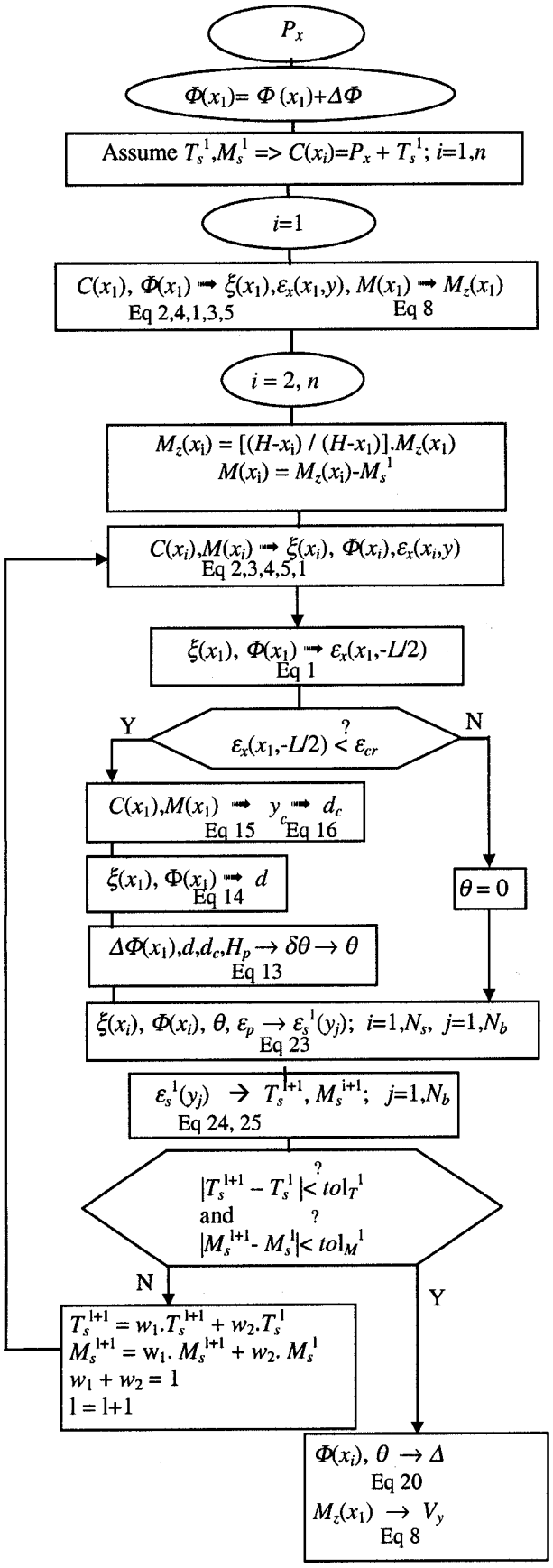

Figure 4—Flowchart of Solution Algorithm for Hysteretic Force-displacement Response

Displacement Controlled Quasi-static Cyclic Analysis of Test Specimens

The numerical solution procedure presented in the foregoing development was implemented to predict the force-displacement hysteresis response of the wall Specimens 2, 3 and 4 tested under lateral in-plane cyclic loading. The analysis was performed incrementally for cyclically increasing and decreasing control curvatures at the base of the shear wall model. The cracking strength of masonry f_{cr} was taken as 5% of the compressive strength f'_m. Because of the absence of lateral bracing along the unbonded length, the yield strength f_{yc} of the unbonded reinforcing bars in compression was assumed to be zero.

Comparison of Analytical Predictions with Test Results

The theoretically calculated cyclic force-displacement relationships are compared with the experimentally observed hysteresis loops for test Specimen 2 in Figure 6 under different axial loads. Similar comparisons are shown for wall Specimens 3 and 4 in Figures 7 and 8 respectively. The figures also show the axial load on the wall specimen and prestrain in the unbonded rebars for the experimental test. For analysis purposes, the average height of the stressed zone H_p was assumed as 0.1 H for 31 kN (697 lbs) axial load and 0.4 H for 116 kN (26,077 lbs) and 205 kN (46,084 lbs) axial load. The peak strength (prism strength) of masonry was scaled down for analyzing the force-displacement envelope under 116 kN (26,077 lbs) axial loads in order to account for strength degradation due to prior cyclic loading of the test specimens under the 31 kN (697 lbs) axial load. The reduction factors for scaling the peak strength were estimated from the deterioration of strength observed in the test specimens in the course of testing under 31 kN (697 lbs) axial load. In case of test Specimen 2, the peak strength was further scaled down for analyzing the response under 205 kN (46,084 lbs) axial load. The scaling factor was estimated from the strength degradation observed during the preceding tests.

The comparisons with the experimental results indicate that the proposed analytical model predicts the hysteretic behavior of concrete masonry shear walls with unbonded reinforcement to a reasonable degree of accuracy. The discrepancies may result from the approximations introduced by underlying assumptions of the modified fiber model. The limitations of these basic assumptions have been discussed previously by Madan et al. (1996). An additional limitation is that the assumed cyclic constitutive relationship for masonry is piece-wise linear, which accounts for the lesser smoothness in the predicted force-displacement response as compared to the observed response. Further, the assumption that plane sections remain plane [Assumption (a)] may limit the accuracy of the model for analysis of

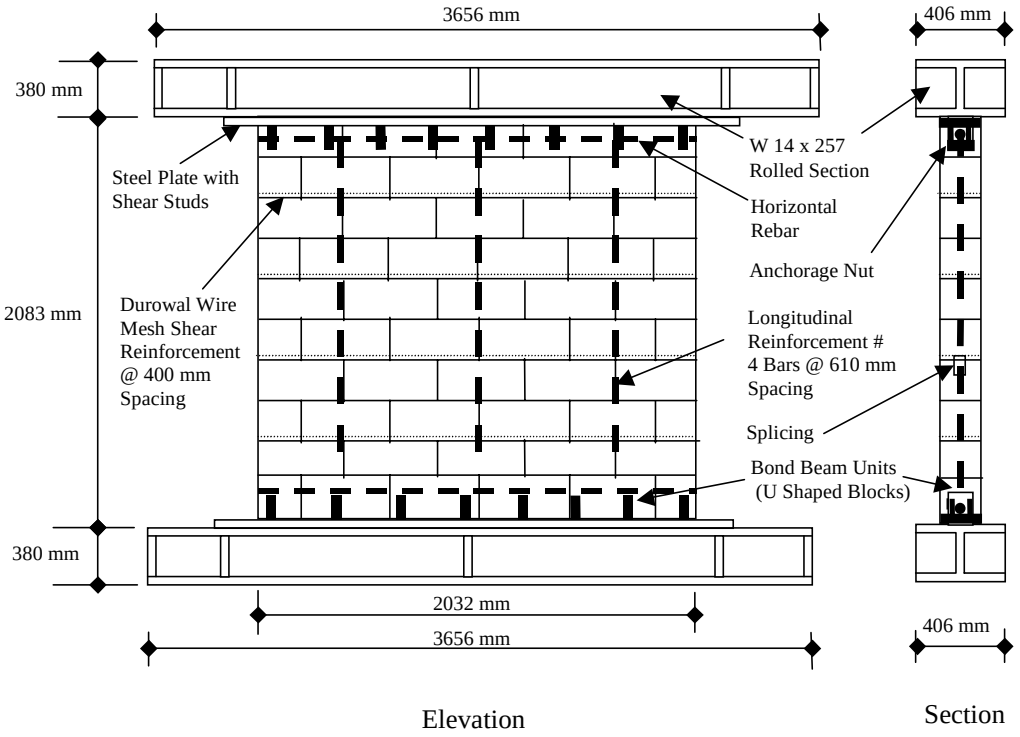

Figure 5—Test Specimen – Typical Details

walls with aspect ratios in the range of 1.0, which is the range of transition from predominant flexural behavior exhibited by slender walls (walls with large aspect ratios) to dominant shear behavior displayed by squat walls (walls with small aspect ratios) [Shing et al. (1989)].

CONCLUSIONS

An analysis technique based on a fiber element model (micro-element model) is presented for evaluating the hysteretic force-displacement behavior of masonry walls with unbonded longitudinal reinforcement under lateral in-plane cyclic loading. The analytical model was used to predict experimental results obtained from cyclic loading tests on wall specimens with unbonded reinforcing bars. The analytically predicted response shows reasonable agreement with the experimentally observed hysteresis behavior. The theoretical model presented in this study is based on force equilibrium and displacement compatibility considerations and thus provides a sound analytical approach for estimating the in-plane strength, ductility and hysteretic energy absorption of masonry walls with unbonded reinforcement subjected to reversed cyclic loading. Since the analytical procedure is developed for a shear wall with cantilever end conditions (cantilever wall) and a concentrated lateral load at the free end, the procedure is limited in the present form

Table 1. Summary of Test Parameters and Results (1 mm = 0.0394 in., 1kN = 224.8 lbs)

Spec. No.	Net Wall He ight (mm)	Vertical Reinf. Ratio	Shear Reinf. mm^2/mm	Pretension in Rebars (kN)	Axial Load (kN)	Cracking Load (kN)
(1)	(2)	(3)	(4)	(5)	(6)	(7)
2	2286	0.026	31/406	0.00	31	11.703
					116	cracked
					205	cracked
3	2286	0.026	31/406	47.37	31	11.587
4	2286	0.026	31/406	94.74	31	9.425
					116	cracked

to such cantilevers walls only. However, the modeling approach is generalized and the proposed model can be easily modified for different boundary conditions, loading patterns and constitutive relationships. The model can be readily adapted for analyzing the hysteretic response of masonry shear walls with bonded reinforcement as well. The proposed modeling technique, therefore, enables rational treatment of various governing factors in a versatile manner.

REFERENCES

Badawi, H. E. S., "Seismic Behavior of Unanchored Liquid Storage Tanks," Ph.D Thesis, Department of Civil Engineering, University of California, Irvine, California, 1989.

Haroun, M. A., "Dynamic Analyses of Liquid Storage Tanks," EERL 80-04, Earthquake Engineering Research Laboratory, California Institute of Technology, Pasadena, CA, Feb 1980.

Haroun, M. A. and Ellaithy, H. M., "Model for Flexible Tanks Undergoing Rocking," Journal of Engineering Mechanics, Vol. 11, No. 2, ASCE, pp.143-157, Feb 1985.

Haroun, M. A. and Housner, G. W., "Dynamic Interaction of Liquid Storage Tanks and Foundation Soil", Proceedings of the Second ASCE/EMD Speciality Conference on Dynamic Response of Structures, Atlanta, GA, pp. 346-360, Jan 1981.

Housner, G. W., "Dynamic Pressures on Accelerated Fluid Containers," Bulletin of Seismological Society of America, Vol. 47, No. 1, pp. 15-35, 1957.

Madan, A., "Nonlinear Modeling of Masonry Walls for Planar Analysis of Building Structures," Ph. D Dissertation, Department of Civil Engineering, State University of New York, Buffalo, March 1996.

Madan, A., Reinhorn, A. M. and Mander, J. B., " Flexural Behavior of Reinforced Masonry Shear Walls with Unbonded Reinforcement," The Masonry Journal, The Professional Journal of Masonry Society, Vol. 14, No. 1, pp. 87-98, August 1996.

Natsiavas, S., "An Analytical Model for Unanchored Fluid-Filled Tanks Under Base Excitation," Journal of Applied Mechanics, Transactions of the ASME, Vol. 55, pp. 648-653, Sept 1988.

Natsiavas, S. and Babcock, C. D., "Behavior of Unanchored Fluid-Filled Tanks Subjected to Ground Excitation," Journal of Applied Mechanics, Transactions of the ASME,, Vol. 55, pp. 654-659, Sept 1988.

Park, R. and T. Paulay, "Reinforced Concrete Structures", John Wiley & Sons, New York, 1975.

Paulay, T. and Priestley, M. J. N., "Seismic Design of Reinforced Concrete and Masonry Buildings," John Wiley & Sons, New York, 1992.

Priestley, M. J. N., Seismic Assessment of Existing Concrete Bridges," University of California, San Diego, Structural Systems Research Report, Report No. SSRP 91/03, 1991.

Shing, P. B., Noland, J. L., Klamerus, E. and Spaeh, H., "Inelastic Behavior of Concrete Masonry Shear Walls," Journal of Structural Engineering, Vol. 115, No. 9, ASCE, pp. 2204 – 2225, September 1989.

`Yi, W. and Natsiavas, S., "Seismic Response of Unanchored Fluid-Filled tanks using Finite Elements," Journal of Pressure Vessel Technology, Transactions of the ASME, Vol 114, pp. 74-79, Feb 1992.

Yield Load (kN)	Ultimate Load (kN)	Cracking Displ. (mm)	Yield Displ. (mm)	Max. Displ. (mm)	Initial Stiffness (kN/mm)	Loading Method
(8)	(9)	(10)	(11)	(12)	(13)	(14)
42.768	63.077	0.229	3.505	28.448	51.768	Inplane drift controlled.
40.939	70.447	cracked	2.591	48.260	15.864	Sinusoidal drift
36.345	70.358	cracked	0.203	28.448	176.654	history@0.1 & 0.2 Hz.
32.110	64.194	0.178	1.854	42.418	65.168	Inplane drift controlled. Sinusoidal drift history@0.1 Hz.
38.867	58.629	0.203	1.372	21.488	45.813	Inplane drift controlled.
50.164	74.192	cracked	1.854	21.488	27.054	Sinusoidal drift history@0.1 & 0.02 Hz.

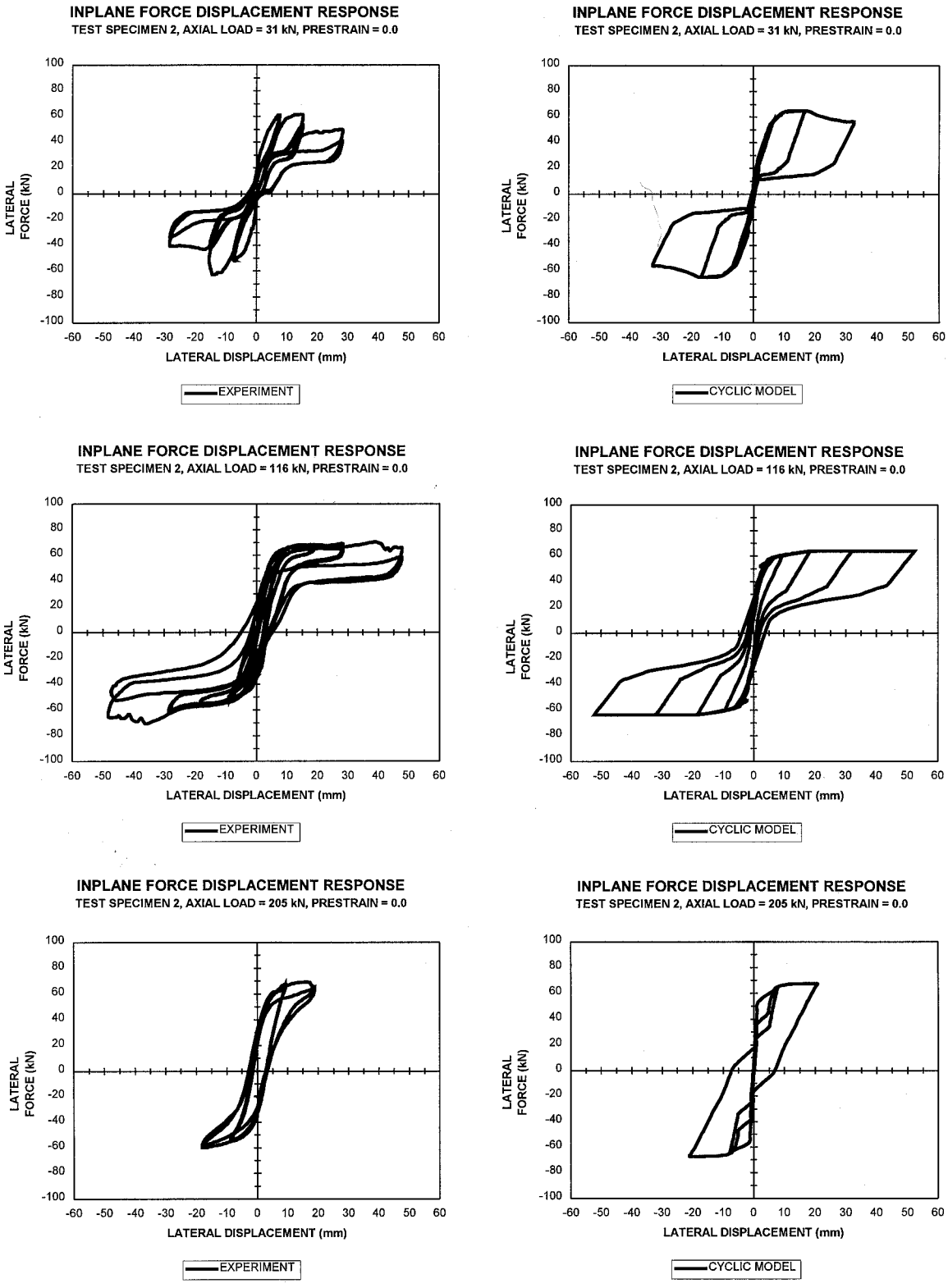

Figure 6—Theoretical vs. Experimental Cyclic Force-Displacement Response for Unbonded Reinforced Masonry Wall Test Specimen 2 (1 kN = 224.8 lbs and 1 mm = 0.0394 in.)

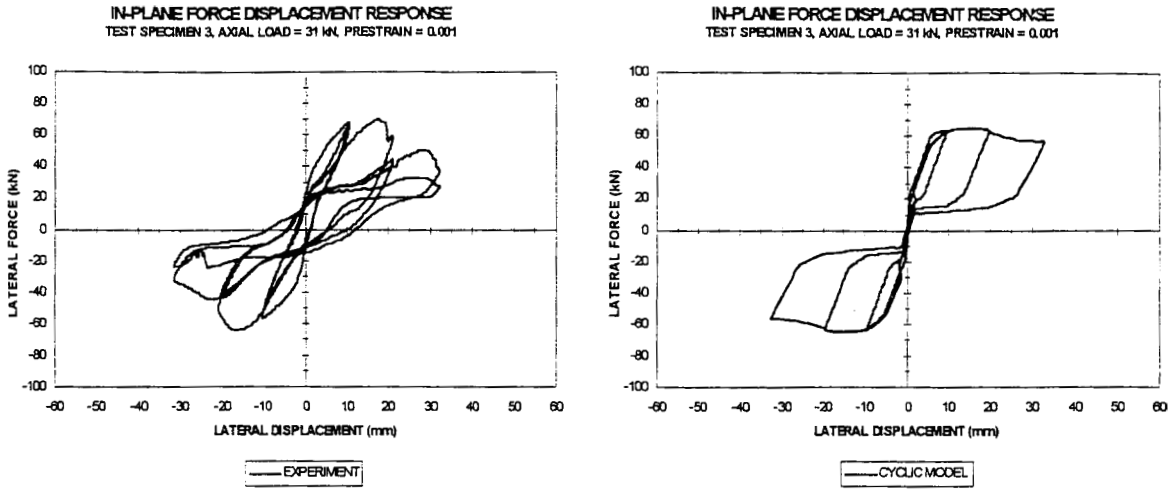

Figure 7—Theoretical vs. Experimental Cyclic Force-Displacement Response for Unbonded (1 kN = 224.8 lbs and 1 mm = 0.0394 in.)

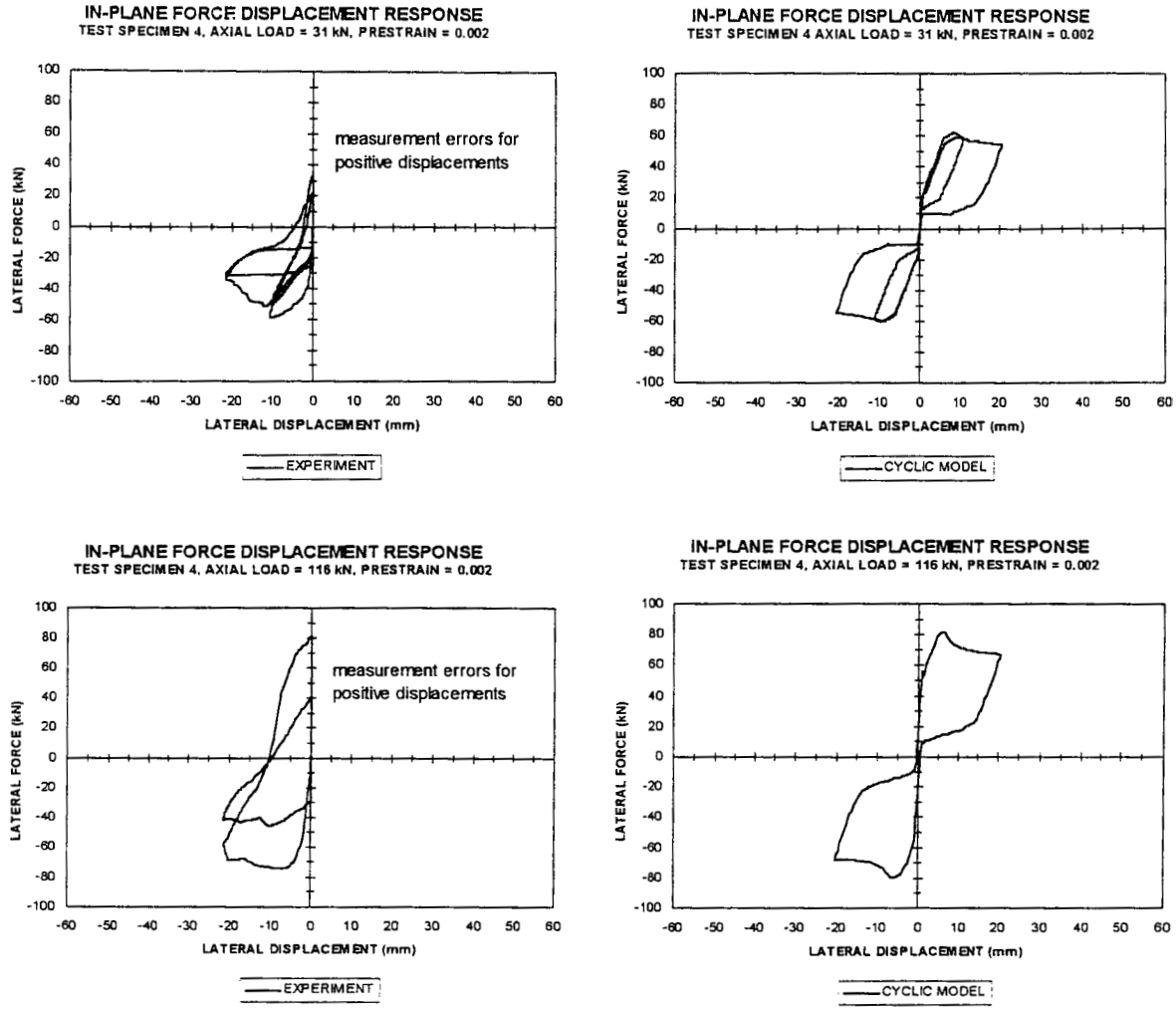

Figure 8—Theoretical vs. Experimental Cyclic Force-Displacement Response for Unbonded Prestressed Masonry Wall Test Specimen 4 (1 kN = 224.8 lbs and 1 mm = 0.0394 in.)

NOTATIONS

A_{sj} = cross-sectional area of the j^{th} steel reinforcing bar.
b = effective width of shear wall.
$C(x_i)$ = internal axial compressive force in masonry at the i^{th} section.
d = length of the contact region at the wall base.
d_c = in-plane distance of point of action of compressive resultant at base from extreme compression fiber (toe of wall).
$E_m(\varepsilon_m)$ = stress-strain relationship for masonry.
$E_m(\varepsilon_s)$ = stress-strain relationship for vertical steel.
f = flexural response parameter.
f_{cr} = cracking stress of masonry.
f'_m = masonry prism strength.
f_y = yield strength of vertical reinforcing steel.
H = effective height of point of application of lateral load V_y from the base.
H_p = average height of stressed region (stress penetration) due to uplift.
i = index for numbering of discrete sections.
j = index for numbering of longitudinal steel bars.
k = index for numbering of discrete steel fibers.
L = length of the wall equal to the depth of a cross-section.
$M(x_i)$ = internal in-plane resisting moment due to masonry at the i^{th} section.
$M_s(x_i)$ = internal in-plane resisting moment due to steel at the i^{th} section.
$M_z(x_i)$ = external bending moment on i^{th} wall section.
n = number of finite sections considered along the height.
n_b = number of vertical steel reinforcing bars.
n_f = number of masonry fibers considered at the given section.
P_x = vertical or axial load on shear wall.
r = rigid body uplift or rocking response parameter.
t_k = thickness of the k^{th} fiber.
$T_s(x_i)$ = internal axial tensile force in steel at the i^{th} section.
$u(x, y)$ = displacement in x direction at location y in i^{th} section.
V_y = in-plane external shear force acting on i^{th} section.
$v(x, y)$ = displacement in y direction at location y in i^{th} section.
w_i = numerical weight factors.
x_i = x coordinate of the i^{th} section.
y_j = y coordinate of the j^{th} bar.
Δ = in-plane lateral displacement at top of the wall.
$\partial\delta_c$ = incremental strain displacements at the wall toe (extreme compression fiber).
$\partial\theta_\delta$ = incremental angle of uplift between uplifted base and foundation.
ε_{cr} = cracking strain of masonry.
$\varepsilon_m(x_i, y)$ = Masonry strain variation along the y axis at i^{th} section.
ε_p = prestressing strain in the vertical steel reinforcing bars.
$\varepsilon_s(x_i, y_j)$ = strain in the j^{th} steel reinforcing bar at the i^{th} section.
$\varepsilon_s(y_j)$ = constant strain in the j^{th} reinforcing bar in case of no bonding.
$\varepsilon_x(x_i, y)$ = normal strain in x direction at location y in i^{th} section.
$\phi(x_i)$ = angle of inclination of the masonry strain profile at the i^{th} section.
θ = angle of rigid body rotation of wall due to uplift.
$\xi(x_i)$ = masonry strain at the center of the i^{th} section = $\varepsilon_m(x_i, 0)$